JACS
JOURNAL OF THE AMERICAN CHEMICAL SOCIETY
Article
pubs.acs.org/JACS

High and Temperature-Insensitive Piezoelectric Strain in Alkali Niobate Lead-free Perovskite

Mao-Hua Zhang,[†] Ke Wang,[*,†] Yi-Jia Du,[‡] Gang Dai,[*,‡] Wei Sun,[†] Geng Li,[†] Duan Hu,[†] Hao Cheng Thong,[†] Chunlin Zhao,[†] Xiao-Qing Xi,[†] Zhen-Xing Yue,[†] and Jing-Feng Li[†]

[†]State Key Laboratory of New Ceramics and Fine Processing, School of Materials Science and Engineering, Tsinghua University, Beijing 100084, P. R. China

[‡]Microsystem and Terahertz Research Center, China Academy of Engineering Physics, Chengdu 610200, P. R. China

Supporting Information

ABSTRACT: With growing concern over world environmental problems and increasing legislative restriction on using lead and lead-containing materials, a feasible replacement for lead-based piezoceramics is desperately needed. Herein, we report a large piezoelectric strain (d_{33}*) of 470 pm/V and a high Curie temperature (T_c) of 243 °C in $(Na_{0.5}K_{0.5})NbO_3$-$(Bi_{0.5}Li_{0.5})TiO_3$-$BaZrO_3$ lead-free ceramics by doping MnO_2. Moreover, excellent temperature stability is also observed from room temperature to 170 °C (430 pm/V at 100 °C and 370 pm/V at 170 °C). Thermally stimulated depolarization currents (TSDC) analysis reveals the reduced defects and improved ferroelectricity in MnO_2-doped piezoceramics from a macroscopic view. Local poling experiments and local switching spectroscopy piezoresponse force microscopy (SS-PFM) demonstrates the enhanced ferroelectricity and domain mobility from a microscopic view. Distinct grain growth and improvement in phase angle may also account for the enhancement of piezoelectric properties.

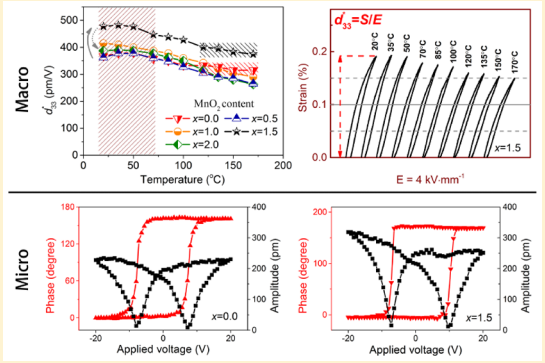

INTRODUCTION

Piezoelectric materials can achieve interconvertibility of the energy between the mechanical and the electrical one. The versatility of $Pb(Zr,Ti)O_3$ (PZT) makes it outshine any other piezoelectric materials and irreplaceable in the global piezoelectric market. Since Saito et al. achieved a PZT-like value of piezoelectric coefficients in $(K,Na)NbO_3$-based (KNN) lead-free ceramics,[1] scientific research in the quest to expel toxic substances represented by PZT has never ceased in the piezoelectric community for the past decade.[2−18] However, PZT is still a monopoly in industry up to now, and is reported to have grasped 94.5% of the piezoactuators market share in 2014.[19]

KNN-based piezoelectric materials are featured with the low driving voltage comparable to that of PZT and thus limited hysteresis and energy dissipation.[4] This characteristic meets the demand for practical applications and in favor of a smooth transition to a lead-free era. Thus, KNN has long been considered as a very promising candidate to replace PZT in certain application fields.[4] In 2016, Wu et al. reported a KNN system with a giant piezoelectric coefficient d_{33}, which is the highest value recorded using a conventional solid-state method and comparable to that of PZT. Apart from the piezoelectric coefficient d_{33}, there are also some other figures of merit when it comes to practical applications, e.g., electromechanical coupling factor k_p and mechanical quality factor Q_m, for transducer applications; piezoelectric strain d_{33}*, for piezoactuator applications. However, a gap still exists between KNN-based piezoeceramics and PZT in terms of the piezoelectric strain d_{33}*.[20,21] Besides, bound by a polymorphic phase transition (PPT) other than the morphotropic phase boundary (MPB) in PZT, KNN-based material usually comes with an inferior temperature stability compared with PZT. Persistent efforts have been made to promote piezoelectricity and stability. For instance, recent studies have unveiled a notable role of zirconium in tailoring R-T phase boundaries, mimicking the MPB structure in the PZT system. And it is generally accepted as a feasible approach to acquire giant piezoelectricity in the KNN system.[2,3,17,22−24] On the basis of previous research and taking a step further by adding manganese, a KNN-based lead-free material with the nominal composition $(Na_{0.5}K_{0.5})$-NbO_3-$(Bi_{0.5}Li_{0.5})TiO_3$-$BaZrO_3$-$x$$MnO_2$ (abbreviated as KNN-BLT-BZ-xMn) is presented. A large piezoelectric strain (d_{33}*) of 470 pm/V is realized, which is comparable to that of PZT, together with a high Curie temperature (T_c) of 243 °C. Moreover, a d_{33}* value of 430 pm/V is maintained until 100 °C, manifesting excellent temperature stability. TSDC and PFM analysis reveal the reduced defects and improved ferroelectricity and domain mobility from the perspective of macroscopic and microscopic views, respectively. In addition,

Received: January 16, 2017
Published: February 24, 2017

DOI: 10.1021/jacs.7b00520
J. Am. Chem. Soc. 2017, 139, 3889−3895

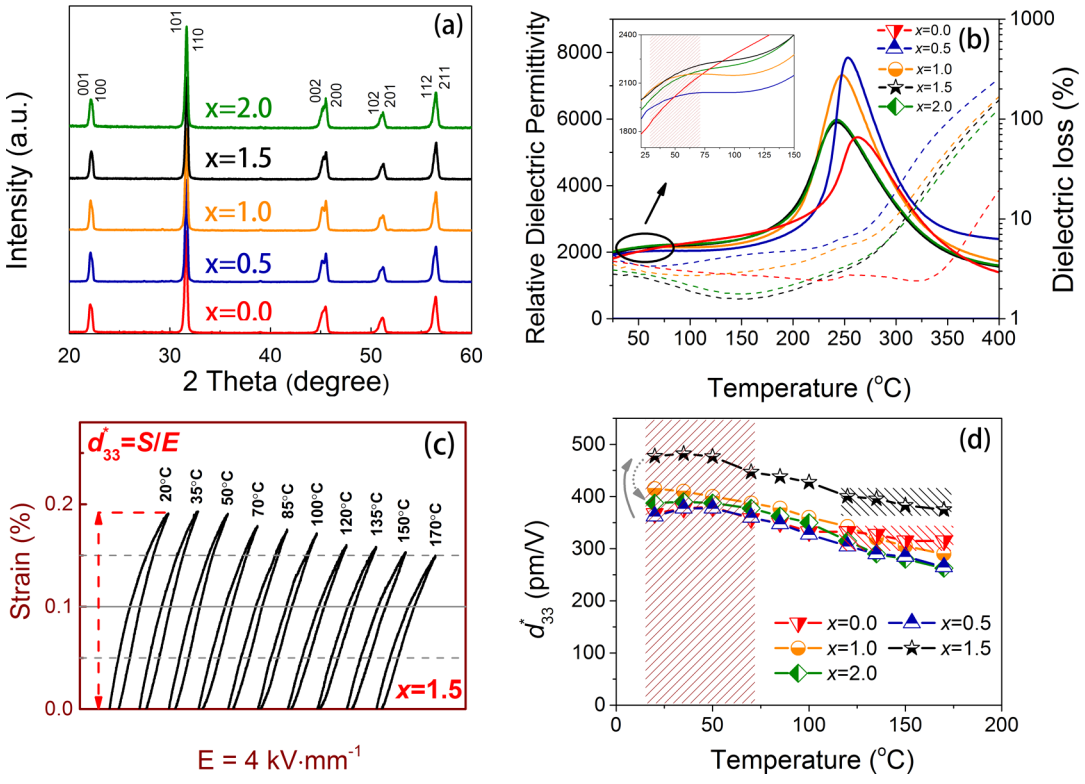

Figure 1. (a) XRD patterns in in the 2θ range 20°−60°. (b) Temperature-dependent dielectric constant and loss of unpoled KNN-BLT-BZ-xMn (x = 0.0−2.0) ceramics. (c) Temperature-dependent unipolar strain curves of KNN-BLT-BZ-xMn (x = 1.5) ceramic. (d) Temperature-dependent large signal d_{33}* of KNN-BLT-BZ-xMn (x = 0.0−2.0) ceramics, measured at 1 Hz, from room temperature to 170 °C.

distinct grain growth and improvement in phase angle may also play a part in the enhancement of piezoelectric properties.

EXPERIMENTAL SECTION

The lead-free ceramics with the nominal composition $0.92(Na_{0.5}K_{0.5})$-NbO_3-$0.02(Bi_{0.5}Li_{0.5})TiO_3$-$0.06BaZrO_3$ + x wt % MnO_2 (In the following termed KNN-BLT-BZ-xMn with x = 0.0, 0.5, 1.0, 1.5, and 2.0) were prepared by the conventional solid-state reaction route described elsewhere.[25] The raw powders were Na_2CO_3, K_2CO_3, Nb_2O_5, Bi_2O_3, Li_2CO_3, TiO_2, $BaCO_3$, and ZrO_2. High-resolution X-ray diffraction (XRD) measurement was utilized to determine the crystal structure using Cu Kα radiation (Rigaku, D/Max2500, Tokyo, Japan). A detailed analysis on microstructures was performed using a scanning electron microscope (SEM, JSM-6460LV, JEOL, Tokyo, Japan). The impedance and phase angle spectra were determined using an impedance analyzer (HP 4294A, Palo Alto, CA). Temperature-dependent dielectric permittivity was measured with an impedance analyzer (TH2827, Changzhou Tonghui Electronic Co, China). A quasi-static piezoelectric constant apparatus was used to determine the piezoelectric coefficient d_{33}. Field-dependent and temperature-dependent parameters including $d_{33}(E)$ hysteresis loops, polarization $P(E)$ hysteresis, bipolar strain $S(E)$, and unipolar strain $S(E)$ were measured with ferroelectric measuring equipment (aixACCT TF Analyzer 1000, Germany). A thermally stimulated depolarization current measurement was conducted using an electrometer/high resistance meter (KEITHLEY 6517B; Keithley Instruments, Inc., Cleveland, OH). Temperature data were collected by the quatro temperature controller of Novocontrol Technologies. The piezoelectric response was characterized using an atomic force microscope (AFM, MFP-3D, Asylum Research, USA) with a functionality of a piezoresponse force microscope (PFM) for the local poling experiments and switching spectroscopy.

RESULTS AND DISCUSSION

Figure 1a shows the X-ray diffraction patterns of KNN-BLT-BZ ceramics modified with different doping amounts of MnO_2, and all the ceramics present typical perovskite structure. Analysis on the relative intensities of (002) and (200) peaks and XRD full-pattern fitting reveal the coexistence of rhombohedral and tetragonal phases.[17,25] To further characterize the phase structure, experiments on the temperature-dependent dielectric constant and dielectric loss (at 1 kHz) of KNN-BLT-BZ-xMn ceramics were performed, as presented in Figure 1b. The dielectric constant anomalies around 250 °C for all the samples correspond to the Curie temperature T_c, representing the phase transition from cubic to tetragonal in the cooling run. Around room temperature, a bump was observed in the dielectric permittivity curve for each composition, which is associated with the R-T phase transition. The corresponding curves are enlarged in the inset, showing typical diffusion behavior in the temperature range from approximately 25 to 70 °C, depending on the specific composition. A similar phenomenon has been observed in $CaZrO_3$-modified KNN piezoceramics, which was speculated to be associated with intergranular stress around polymorphic phase transitions[26] and could possibly act as a key factor for obtaining enhanced thermal stabilities in KNN-based materials.[5] The incorporation of ABO_3-type perovskites $(Bi_{0.5}Li_{0.5})TiO_3$ and $BaZrO_3$, which decreases the O-T phase transition temperature ($T_{O\text{-}T}$) and increases the R-O phase transition temperature ($T_{R\text{-}O}$) simultaneously, leads to the formation of the R-T phase boundary at ambient temperature. The accompanying existence of 14 possible directions for polarization orientations around the boundary (8 from the rhombohedral and 6 from the tetragonal) can exert influence on the polarization mechanism and may account for the

DOI: 10.1021/jacs.7b00520
J. Am. Chem. Soc. 2017, 139, 3889−3895

diffusion. Furthermore, the diffusion phenomenon is possibly due to the relaxor behavior observed in all compositions (Figure S6: Relaxor characteristic of the KNN-BLT-BZ-xMn). Compared with the ceramics without MnO_2 doping, it can be noticed that the ceramics with MnO_2 doping have a lower T_c. The peak value of the dielectric constant at T_c increases from 5455 at x = 0.0 to a maximum value of 7847 at x = 0.50 and then slightly decreases to the value of 5900 at x = 2.0, revealing that the spontaneous polarization of these samples first increased and then decreased with the increasing x.[27] Moreover, the dielectric constant at room temperature increases with increasing x, reaching a maximum at x = 1.5, and then decreases slightly. At the same time, the room temperature dielectric losses are lowered with increasing MnO_2 addition (see Table S1, Electrical properties of KNN-BLT-BZ-xMn ceramics).

Well-defined $P(E)$ hysteresis loops are observed for all the measured samples (Figure S1a: $P(E)$ loops of KNN-BLT-BZ-xMn ceramics), revealing their ferroelectric properties, which are not strongly dependent on the MnO_2 contents. Ceramics with MnO_2 doping exhibit square-like hysteresis loops with lower coercive field E_c. To fully understand the composition-dependent ferroelectric properties, both P_r and E_c are plotted as a function of MnO_2 content x (Figure S1c: Remnant polarization P_r and coercive field E_c of KNN-BLT-BZ-xMn ceramics). P_r grows with the increasing x, reaching a maximum of 16.4 $\mu C/cm^2$ at x = 1.0. Then, it declines to 15.8 and 15.2 $\mu C/cm^2$ as x increases to 1.5 and 2.0, respectively. E_c is reduced from 1.30 kV/mm to 1.08 kV/mm, owing to the addition of MnO_2 (x = 0.5), and then it remains in the lower range of 1.10−1.19 kV/mm with the further increase of x. The ferroelectric properties of the ceramics are promoted with the addition of MnO_2, which is associated with the enhanced domain mobility and easier polarization switching boosted by the reduced E_c. Typical butterfly shape strain curves are observed for all the ceramics with different MnO_2 doping (Figure S1b: bipolar strain $S(E)$ curves of KNN-BLT-BZ-xMn ceramics). The magnitude of S_{neg} is associated with the competitions between 180° and non-180° ferroelectric domains switching; that is, the more the non-180° domain switching, the greater the value is.[19] It also represents the reversible domain switching of piezoceramics harvested under electrical field excitation, which can be regarded as the ferroelectricity contribution. So the improved S_{neg} also implies enhanced ferroelectricity with the addition of MnO_2, which is in agreement with P_r.

Temperature-dependent piezoelectric strain curves of KNN-BLT-BZ-xMn (x = 1.5) ceramics are exemplified in Figure 1c. The strain that is repeatedly harvested in unipolar conditions is approximately equal to the S_{pos} in bipolar conditions (Figure S1b: bipolar strain $S(E)$ curves of KNN-BLT-BZ-xMn ceramics), which is a figure of merit in practical actuator applications. The normalized strain $d_{33}^*(S_{max}/E_{max})$ shares the same unit (pm/V or pC/N) with piezoelectric coefficient d_{33}, but is adopted on occasion under large field excursions.[30] d_{33}^* is usually referred to as a large signal property while the value obtained through the quasi-static piezoelectric constant apparatus is called small signal d_{33}. To investigate the influence of MnO_2 on the piezoelectric strain behaviors of KNN-BLT-BZ-xMn ceramics, temperature-dependent large signal d_{33}^* values were calculated from piezoelectric strain curves and plotted in Figure 1d. At room temperature, d_{33}^* increases largely with the increasing x, giving a maximum value of 470 pm/V at x = 1.5. This property is superior among KNN-based lead-free piezoceramics and also comparable to that of soft PZT PIC151, as listed in Table 1. Surprising temperature stability is observed for all the compositions from room temperature to 70 °C, which is supposed to be boosted by the diffused phase transition existing in this very range (as shown in the left shadow).[5] Note that the ceramic with composition x = 0 shows good temperature stability in the whole temperature range from room temperature to 170 °C. More surprisingly, the ceramics with composition x = 1.5 exhibit excellent d_{33}^* performance together with outstanding temperature stability. Furthermore, it is noted that the d_{33}^* variation of our material in the range from room temperature to 100 °C is less than −10% of its room-temperature value, which is indicated by shadows in Figure S7 (Comparison of temperature dependence of large signal d_{33}^* for various piezoceramics as normalized to its room temperature value $d_{33}^*{}_{RT}$). The temperature stability of the piezoelectric performance is much better than that of other representative KNN-based ceramics and commercial PZT5H ceramics, even comparable to the well-known PZT4 ceramics, which are suitable for applications requiring stable outputs.[1,31−33]

Table 1. Piezoelectric Strain d_{33}^* under Certain Electric Fields and Curie Temperature of Representative Systems

System	d_{33}^* (pm/V)	E (kV/mm)	T_c (°C)	Reference
KNN-BLT-BZ-1.5MnO_2	475	4	243	This work
LF4 (KNN-based)	400	2	256	*Nature*[1]
CZ5 (KNN-based)	357	4	200	*Adv. Funct. Mater.*[5]
KNNS-BNKZ (KNN-based)	355	4	267	*ACS Appl. Mater. Interface*[28]
BNT-BT-ZnO (BNT-based)	110	6	280	*Nat. Commun.*[29]
BNT-BT-KNN (BNT-based)	560	8		*Appl. Phys. Lett.*[10]
PIC151 (Soft PZT)	500		250	*Appl. Phys. Lett.*[10]

The influence of MnO_2 on the room temperature piezoelectric properties (d_{33}, k_p) and the mechanical quality factor (Q_m) is illustrated in Figure S2 (Room temperature piezoelectric properties d_{33}, k_p, and Q_m of poled KNN-BLT-BZ-xMn ceramics). The ceramics with MnO_2 doping possess higher d_{33}, k_p, and Q_m values, and both d_{33} and k_p are optimized at x = 1.5, indicating that this composition is optimal for comprehensive piezoelectric properties. The enhancement of d_{33} and k_p could be regarded as the "softening" effect while that of Q_m can be considered the "hardening" one. The simultaneous occurrence of "softening" and "hardening" effects ignites controversy over the role of MnO_2 played in KNN-based piezoceramics, which has also been reported in many other pieces of literature and is not the subject here.[34−37]

The microstructure and PFM phase images of x = 0 and x = 1.0 samples are shown in Figure 2 as representative, and the surface morphology of all the composition ceramics is also provided (Figure S3: Surface morphology of KNN-BLT-BZ-xMn ceramics). All the ceramics have a dense structure, and the relative densities of all the sintered samples are larger than 95%. For the undoped ceramics, the grain size distribution is broad and the average grain size is relatively small, which is 0.87 μm. The grain size distribution is inhomogeneous, as some of the grains increase and the average grain size becomes larger after adding MnO_2. For the KNN-BLT-BZ-xMn ceramics with x =

DOI: 10.1021/jacs.7b00520
J. Am. Chem. Soc. 2017, 139, 3889−3895

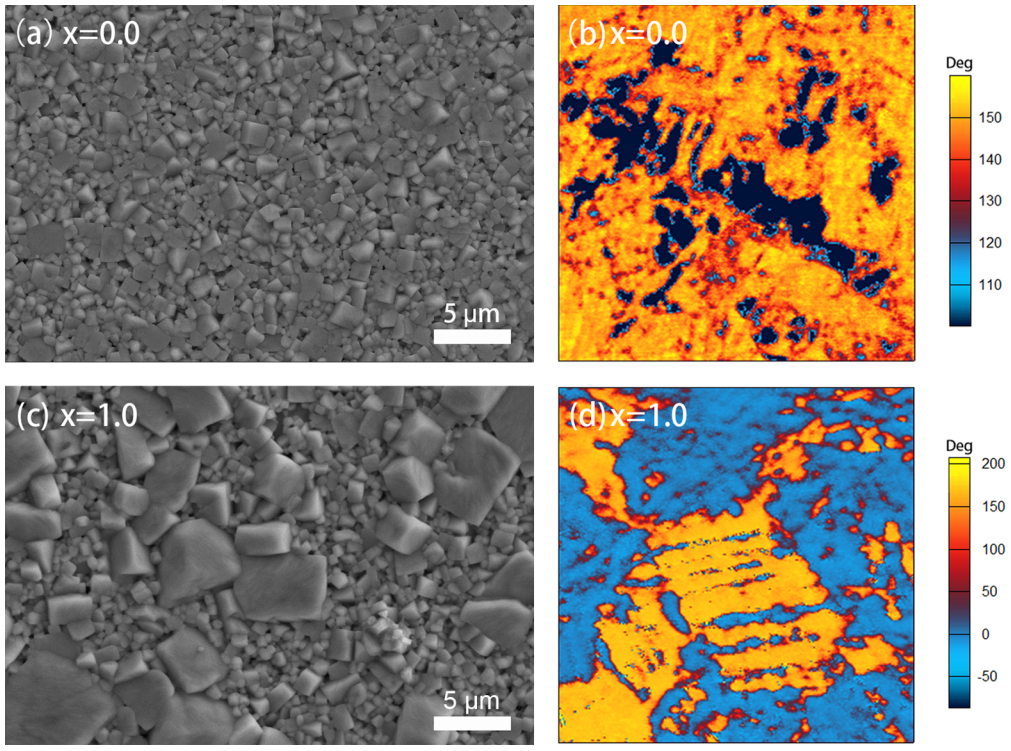

Figure 2. Surface morphology of KNN-BLT-BZ ceramics modified with different MnO_2 contents: (a) x = 0.0, (c) x = 1.0. (b) Vertical piezoresponse force microscopy (PFM) phase image of x = 0.0. (d) Lateral PFM phase image of x = 1.0.

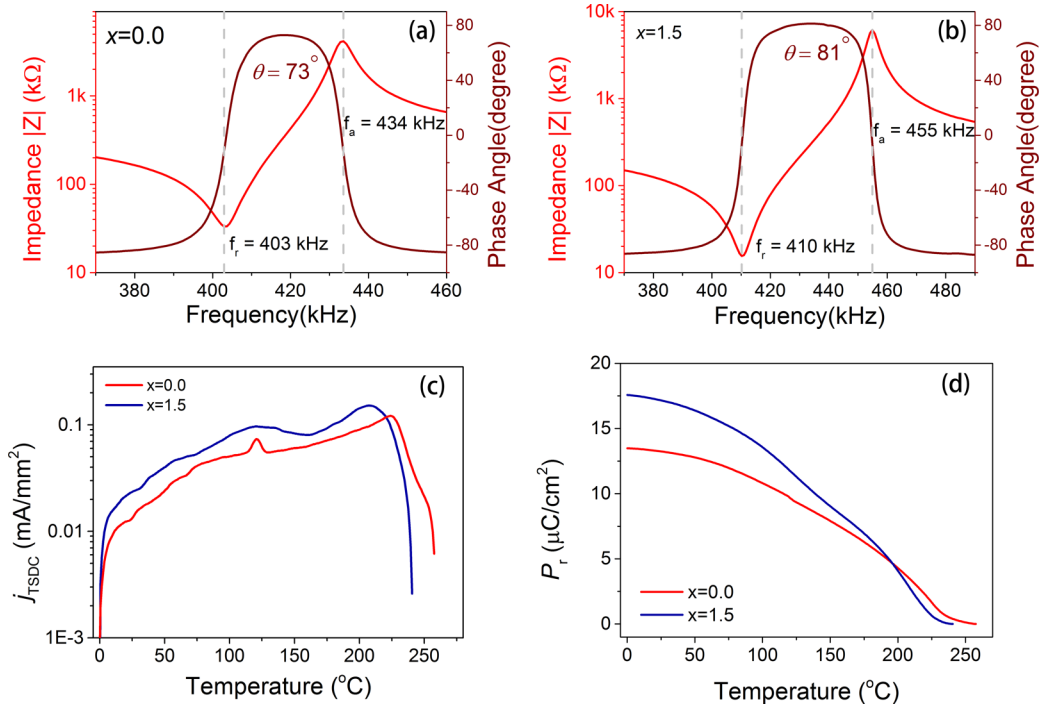

Figure 3. (a, b) Room temperature impedance |Z| and phase angle θ as a function of frequency of KNN-BLT-BZ-xMn (x = 0.0 and x = 1.5) ceramics. (c) Temperature dependence of depolarization current j_{TSDC} and (d) calculated P_r for poled KNN-BLT-BZ-xMn (x = 0 and x = 1.5) samples.

0.5, 1.0, 1.5, and 2.0, the grains have an average size of 1.75 μm, 1.48 μm, 1.60 μm, and 1.39 μm, respectively. The increased grain size may contribute to the enhanced piezoelectric properties as an extrinsic factor, which is also reported in other systems.[35,38] The addition of MnO_2, which may act as a sintering aid by forming a liquid phase, is a possible reason for the grain growth. The sintering temperature decreases gradually with the increasing MnO_2 contents, verifying the effectiveness of MnO_2 in promoting sintering and densification of the ceramics.

DOI: 10.1021/jacs.7b00520
J. Am. Chem. Soc. 2017, 139, 3889−3895

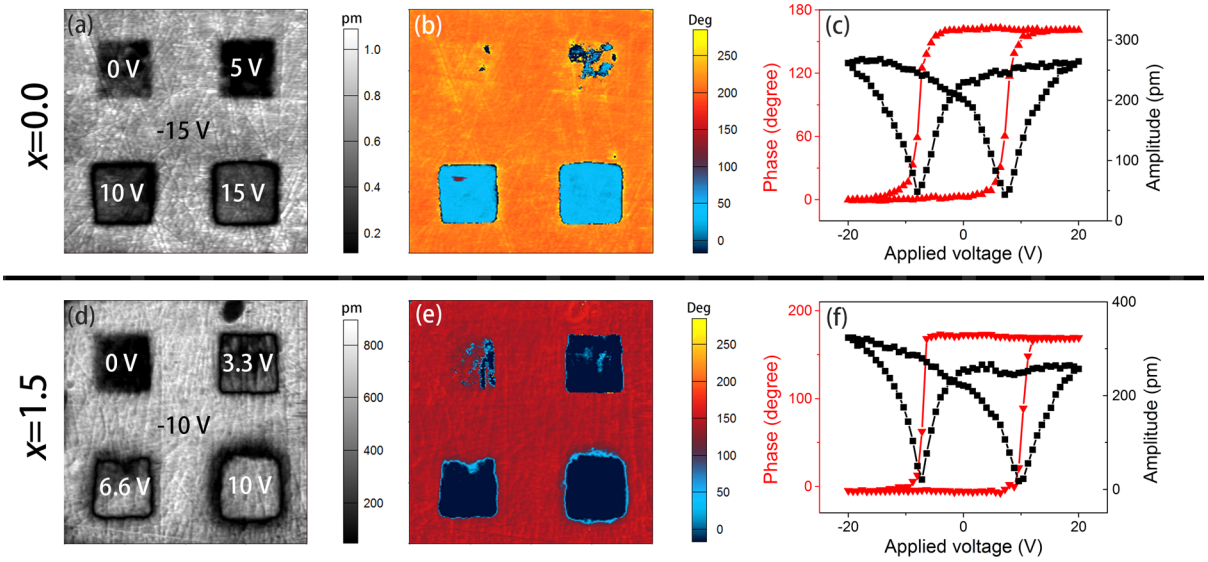

Figure 4. Poling behavior, piezoresponse hysteresis loops, and typical butterfly shaped amplitude−voltage curves of KNN-BLT-BZ-*x*Mn (x = 0 and x = 1.5). Out-of-plane images after poling with different electrical voltages, as illustrated in parts a and d, where the larger and the smaller squares correspond to 4 × 4 μm^2 area and 1 × 1 μm^2 area, respectively.

Note that KNN-BLT-BZ-*x*Mn (x = 1.5) ceramics possess large signal piezoelectric properties with excellent temperature stability. Moreover, the temperature stability of the small signal piezoelectric properties is also noticeable (Figure S5: Temperature-dependent $d_{33}(E)$ hysteresis loops of KNN-BLT-BZ-1.5Mn ceramics and temperature-dependent small signal d_{33} of KNN-BLT-BZ-*x*Mn, x = 0.0, 1.0, and 1.5). The $d_{33}(E)$ hysteresis loops of the x = 1.5 sample are shown, where $d_{33}(E)$ at zero electrical field, $d_{33}(E = 0\ V)$, could be considered as small signal d_{33}. It should be noted that an analogy between the field-dependent $d_{33}(E = 0\ V)$ value of 324 pm/V and the quasi-static d_{33} value of 340 pC/N at room temperature occurs as expected (Table S1, Electrical properties of KNN-BLT-BZ-*x*Mn ceramics).[39] A comparison is made among x = 0, x = 1.0, and x = 1.5 ceramics on the temperature-dependent small signal d_{33}. For all three compositions, d_{33} remains rather stable in the whole temperature range from room temperature to 170 °C, manifesting decent intrinsic piezoelectricity. Moreover, the x = 1.5 sample shows slightly better temperature stability as well as piezoelectric output.

The phase angle θ is a valuable indicator to evaluate the poling state of piezoceramics, which is supposed to approach 90° for an ideally poled sample.[34,40] The impedance magnitude Z and phase angle θ as a function of frequency of the KNN-BLT-BZ-*x*Mn ceramics (x = 0.0 and x = 1.5) are plotted in Figure 3a and 3b. Compared with KNN-BLT-BZ-*x*Mn ceramics without MnO_2 doping, ceramics with MnO_2 doping show higher θ value (Figure S4: room temperature impedance |Z| and phase angle θ as a function of frequency of KNN-BLT-BZ-*x*Mn ceramics), reaching an optimum value of 81 at x = 1.5. The high θ value obtained at $x \geq 1.0$ manifests that, by doping MnO_2 additive, it is easier to pole the ceramics to an optimum state by facilitating domain orientation, leading to an enhancement of the piezoelectric coefficient d_{33}. Thermally stimulated depolarization currents (TSDCs) are regarded as a powerful tool to study and characterize the defects that may exist in the dielectric materials.[41−43] The temperature dependence of the depolarization current j_{TSDC} and the integral calculated P_r for poled KNN-BLT-BZ-*x*Mn (x = 0 and x = 1.5) samples are shown in Figure 3c and 3d. A TSDC relaxation peak is observed in the x = 0.0 sample, which may be associated with the migration of oxygen vacancies.[43,44] However, no peak is observed in MnO_2-doped ceramics. As x = 0.0 ceramics were sintered at a very high temperature of 1200 °C, alkaline volatilization possibly occurred, resulting in nonstoichiometry and defect, e.g. oxygen, vacancies. For MnO_2-doped ceramics, the volatilization of alkaline elements may be compensated by manganese, due to its multiple accessible valence states, leading to reduction of oxygen vacancy defects.

Note that the remnant polarization P_r of the x = 1.5 sample is higher than that of x = 0 in the whole temperature range from room temperature to 170 °C. Considering the limited difference in the relative dielectric permittivity between the two compositions in this very temperature range, the improved intrinsic piezoelectric response (proportional to the product of P_r and the relative dielectric permittivity) contributes to the better piezoelectric coefficient as well as temperature stability. The additive of MnO_2 effectively reduces the defects and boosts the ferroelectricity in the piezoceramics, leading to an improvement in the piezoelectric properties and temperature stability.

Piezoresponse force microscopy (PFM) provides insight into the piezoelectric properties from a microscopic point of view.[32,45−48] Two samples, KNN-BLT-BZ-*x*Mn (x = 0.0 and 1.5) were selected for comparison (Figure 4). To explore the reversibility of the ferroelectric domains, local poling experiments were conducted. A negative DC voltage large enough to induce complete polarization orientation was first applied to the tip during the scanning of a 4 × 4 μm^2 area. Then, a positive DC voltage with different values, depending on the composition, was applied to the tip during the scanning of a 1 × 1 μm^2 area. The out-of-plane (OP) PFM amplitude and phase images of the x = 0.0 sample and the x = 1.5 sample are presented in Figure 4a−b and Figure 4d−e, respectively, as well as the magnitude of the applied voltage. For the x = 0.0 sample, domains have only partially been induced under a voltage of 5 V, which is not sufficient to induce complete domains switching. For x = 1.5, a relatively low voltage of 3.3 V is

DOI: 10.1021/jacs.7b00520
J. Am. Chem. Soc. 2017, 139, 3889−3895

enough to induce sufficient domains reversal, where the square exhibits inverse phase contrast compared to the surrounding part. The reduced voltage to induce complete domain switching in the MnO_2-doped sample is correlated to the enhanced domain mobility, which is observed hereinbefore and has been proved here. To further characterize the piezoelectric properties, the local switching spectroscopy piezoresponse force microscopy (SS-PFM) was employed. A sequence of DC voltage ranging from −20 to 20 V with a superimposed AC signal of 1 V was applied to the sample through the conductive tip during scanning.[49] To ensure the representativeness and reliability of our results, a piezoresponse measurement was performed within a 20 × 20-μm-sized mesh of 100 points. Typical phase hysteresis loops and amplitude-to-voltage curves were shown in Figure 4c and Figure 4f, respectively. Both of the phase curves reveal 180° contrast under the external electrical field, manifesting sufficient polarization switching behavior. It should be noted that the sample with MnO_2 doping exhibits a more square-like hysteresis loop, indicating better ferroelectricity. Both of the samples present complete butterfly shaped piezoresponse curves. The amplitudes of the piezoresponse under zero and the maximum electrical field divided by AC voltage (1 V) are termed as the local effective piezoelectric coefficients d_{33} and d_{max}, respectively. For the $x = 0$ and $x = 1.5$ samples, d_{33} values are 200 and 235 pm/V, respectively, which are comparable to those obtained by testing on bulk ceramics. The microscopic results supported by PFM are in coincidence with those from the macroscopic perspective.

CONCLUSIONS

A large piezoelectric strain d_{33}* of 470 pm/V associated with high temperature-insensitive behavior (a high curie temperature T_c of 243 °C and d_{33}* of 430 pm/V at 100 °C) is reported in alkali niobate lead-free perovskite. MnO_2 doping has significantly boosted the comprehensive piezoelectric and ferroelectric performance through a combination of macro- and microscale methods of property characterization. We believe that properly modified lead-free perovskites are potential substitutes for lead-based counterparts, especially for fields requiring thermally stable piezoelectric output.

ASSOCIATED CONTENT

Supporting Information

The Supporting Information is available free of charge on the ACS Publications website at DOI: 10.1021/jacs.7b00520.

Supporting $P(E)$ and bipolar strain $S(E)$ curves, SEM images, impedance spectroscopy, temperature-dependent small signal d_{33} and large signal d_{33}*, relaxor characteristics, and other electrical properties of KNN-BLT-BZ-xMn (x = 0.0−2.0) ceramics (PDF)

AUTHOR INFORMATION

Corresponding Authors

*wang-ke@tsinghua.edu.cn
*daigang@mtrc.ac.cn

ORCID

Ke Wang: 0000-0001-9840-2427

Notes

The authors declare no competing financial interest.

ACKNOWLEDGMENTS

This work was supported by National Nature Science Foundation of China (Grants no. 51572143, 51332002), the Tsinghua University Initiative Scientific Research Program (Grant no. 20131089230), and Science Challenge Project (No. JCKY2016212A503).

REFERENCES

(1) Saito, Y.; Takao, H.; Tani, T.; Nonoyama, T.; Takatori, K.; Homma, T.; Nagaya, T.; Nakamura, M. *Nature* **2004**, *432* (7013), 84−87.
(2) Wu, B.; Wu, H.; Wu, J.; Xiao, D.; Zhu, J.; Pennycook, S. J. *J. Am. Chem. Soc.* **2016**, *138* (47), 15459−15464.
(3) Wang, X.; Wu, J.; Xiao, D.; Zhu, J.; Cheng, X.; Zheng, T.; Zhang, B.; Lou, X.; Wang, X. *J. Am. Chem. Soc.* **2014**, *136* (7), 2905−10.
(4) Rödel, J.; Webber, K. G.; Dittmer, R.; Jo, W.; Kimura, M.; Damjanovic, D. *J. Eur. Ceram. Soc.* **2015**, *35* (6), 1659−1681.
(5) Yao, F.-Z.; Wang, K.; Jo, W.; Webber, K. G.; Comyn, T. P.; Ding, J.-X.; Xu, B.; Cheng, L.-Q.; Zheng, M.-P.; Hou, Y.-D.; Li, J.-F. *Adv. Funct. Mater.* **2016**, *26* (8), 1217−1224.
(6) Rödel, J.; Jo, W.; Seifert, K. T. P.; Anton, E.-M.; Granzow, T.; Damjanovic, D. *J. Am. Ceram. Soc.* **2009**, *92* (6), 1153−1177.
(7) Shrout, T. R.; Zhang, S. J. *J. Electroceram.* **2007**, *19* (1), 113−126.
(8) Zhang, S.; Xia, R.; Shrout, T. R.; Zang, G.; Wang, J. *J. Appl. Phys.* **2006**, *100* (10), 104108.
(9) Panda, P. K. *J. Mater. Sci.* **2009**, *44* (19), 5049−5062.
(10) Zhang, S.-T.; Kounga, A. B.; Aulbach, E.; Ehrenberg, H.; Rödel, J. *Appl. Phys. Lett.* **2007**, *91* (11), 112906.
(11) Zuo, R.; Qi, H.; Fu, J. *Appl. Phys. Lett.* **2016**, *109* (2), 022902.
(12) Zuo, R.; Fang, X.; Ye, C. *Appl. Phys. Lett.* **2007**, *90* (9), 092904.
(13) Wu, J.; Xiao, D.; Zhu, J. *Chem. Rev.* **2015**, *115* (7), 2559−95.
(14) Li, F.; Zhang, S.; Yang, T.; Xu, Z.; Zhang, N.; Liu, G.; Wang, J.; Wang, J.; Cheng, Z.; Ye, Z. G.; Luo, J.; Shrout, T. R.; Chen, L. Q. *Nat. Commun.* **2016**, *7*, 13807.
(15) Liu, W. F.; Ren, X. B. *Phys. Rev. Lett.* **2009**, *103* (25), 257602.
(16) Hong, C.-H.; Kim, H.-P.; Choi, B.-Y.; Han, H.-S.; Son, J. S.; Ahn, C. W.; Jo, W. *J. Materiomics.* **2016**, *2* (1), 1−24.
(17) Wang, R.; Wang, K.; Yao, F.; Li, J.-F.; Schader, F. H.; Webber, K. G.; Jo, W.; Rödel, J. *J. Am. Ceram. Soc.* **2015**, *98* (7), 2177−2182.
(18) Malič, B.; Koruza, J.; Hrešćak, J.; Bernard, J.; Wang, K.; Fisher, J.; Benčan, A. *Materials* **2015**, *8* (12), 8117−8146.
(19) Jo, W.; Dittmer, R.; Acosta, M.; Zang, J.; Groh, C.; Sapper, E.; Wang, K.; Rödel, J. *J. Electroceram.* **2012**, *29* (1), 71−93.
(20) Haertling, G. H. *J. Am. Ceram. Soc.* **1999**, *82* (4), 797−818.
(21) Park, S.-E.; Shrout, T. R. *J. Appl. Phys.* **1997**, *82* (4), 1804.
(22) Zuo, R.; Fu, J. *J. Am. Ceram. Soc.* **2011**, *94* (5), 1467−1470.
(23) Zhang, B.; Wu, J.; Cheng, X.; Wang, X.; Xiao, D.; Zhu, J.; Wang, X.; Lou, X. *ACS Appl. Mater. Interfaces* **2013**, *5* (16), 7718−25.
(24) Wang, X.; Wu, J.; Xiao, D.; Cheng, X.; Zheng, T.; Zhang, B.; Lou, X.; Zhu, J. *J. Mater. Chem. A* **2014**, *2* (12), 4122.
(25) Zhang, M.-H.; Wang, K.; Zhou, J. S.; Zhou, J. J.; Chu, X.; Lv, X.; Wu, J.; Li, J.-F. *Acta Mater.* **2017**, *122*, 344−351.
(26) Chen, F.; Li, Y.-H.; Gao, G.-Y.; Yao, F.-Z.; Wang, K.; Li, J.-F.; Li, X.-L.; Gao, X.-Y.; Wu, W. *J. Am. Ceram. Soc.* **2015**, *98* (4), 1372−1376.
(27) Watanabe, Y.; Sumida, K.; Yamada, S.; Sago, S.; Hirano, S.-i.; Kikuta, K. *Jpn. J. Appl. Phys.* **2008**, *47* (5), 3556−3558.
(28) Qin, Y.; Zhang, J.; Yao, W.; Lu, C.; Zhang, S. *ACS Appl. Mater. Interfaces* **2016**, *8* (11), 7257−65.
(29) Zhang, J.; Pan, Z.; Guo, F. F.; Liu, W. C.; Ning, H.; Chen, Y. B.; Lu, M. H.; Yang, B.; Chen, J.; Zhang, S. T.; Xing, X.; Rodel, J.; Cao, W.; Chen, Y. F. *Nat. Commun.* **2015**, *6*, 6615.
(30) Chen, X.; Wang, Y.; Chen, J.; Zhou, H.; Fang, L.; Liu, L.; Randall, C. A. *J. Am. Ceram. Soc.* **2013**, *96* (11), 3489−3493.
(31) Zhang, S. T.; Kounga, A. B.; Aulbach, E.; Granzow, T. *J. Appl. Phys.* **2008**, *103* (3), 034107.
(32) Zhou, J.-S.; Wang, K.; Yao, F.-Z.; Zheng, T.; Wu, J.; Xiao, D.; Zhu, J.; Li, J.-F. *J. Mater. Chem. C* **2015**, *3* (34), 8780−8787.

DOI: 10.1021/jacs.7b00520
J. Am. Chem. Soc. 2017, 139, 3889−3895

(33) Wang, D.; Fotinich, Y.; Carman, G. P. *J. Appl. Phys.* **1998**, *83* (10), 5342−5350.
(34) Lin, D.; Kwok, K. W.; Chan, H. L. W. *J. Alloys Compd.* **2008**, *461* (1−2), 273−278.
(35) Liu, Q.; Zhu, F. Y.; Zhao, L.; Wang, K.; Li, L.; Li, J.-F. *J. Am. Ceram. Soc.* **2016**, *99* (11), 3670−3676.
(36) Mgbemere, H. E.; Hinterstein, M.; Schneider, G. A. *J. Am. Ceram. Soc.* **2013**, *96* (1), 201−208.
(37) Ariizumi, T.; Zushi, J.; Kojima, S.; Wang, R.; Bando, H. *Jpn. J. Appl. Phys.* **2012**, *51*, 07GC01.
(38) Randall, C. A.; Kim, N.; Kucera, J. P.; Cao, W. W.; Shrout, T. R. *J. Am. Ceram. Soc.* **1998**, *81* (3), 677−688.
(39) Yao, F. Z.; Yu, Q.; Wang, K.; Li, Q.; Li, J.-F. *RSC Adv.* **2014**, *4* (39), 20062−20068.
(40) Yao, F. Z.; Wang, K.; Jo, W.; Lee, J. S.; Li, J.-F. *J. Appl. Phys.* **2014**, *116* (11), 114102.
(41) Zhang, J.; Yue, Z.; Zhou, Y.; Zhang, X.; Li, L.; Davies, P. *J. Am. Ceram. Soc.* **2015**, *98* (5), 1548−1554.
(42) Zhang, X.; Zhang, Y.; Zhang, J.; Peng, B.; Xie, Z.; Yuan, L.; Yue, Z.; Li, L.; Alan Randall, C. *J. Am. Ceram. Soc.* **2014**, *97* (10), 3170−3176.
(43) Zhang, X.; Yue, Z.; Peng, B.; Xie, Z.; Yuan, L.; Zhang, J.; Li, L.; Randall, C. *J. Am. Ceram. Soc.* **2014**, *97* (9), 2921−2927.
(44) Rojac, T.; Ursic, H.; Bencan, A.; Malic, B.; Damjanovic, D. *Adv. Funct. Mater.* **2015**, *25* (14), 2099−2108.
(45) Li, J.; Li, J.-F.; Yu, Q.; Chen, Q. N.; Xie, S. *J. Materiomics.* **2015**, *1* (1), 3−21.
(46) Dittmer, R.; Jo, W.; Rödel, J.; Kalinin, S.; Balke, N. *Adv. Funct. Mater.* **2012**, *22* (20), 4208−4215.
(47) Yao, F.-Z.; Wang, K.; Cheng, L.-Q.; Zhang, X.; Zhang, W.; Zhu, F.; Li, J.-F. *J. Am. Ceram. Soc.* **2015**, *98* (2), 448−454.
(48) Zhou, J.-S.; Wang, K.; Yao, F.-Z.; Zheng, T.; Wu, J.; Xiao, D.; Zhu, J.; Li, J.-F. *J. Mater. Chem. C* **2015**, *3* (34), 8780−8787.
(49) Sun, W.; Yu, Q.; Li, J.; Li, J.-F. *J. Phys. Chem. C* **2015**, *119* (34), 19891−19896.

DOI: 10.1021/jacs.7b00520
J. Am. Chem. Soc. 2017, 139, 3889−3895